



Experimental Validation of a Gap Damper to Control the Displacement Demands in a Seismically Isolated Building

K. Ryan⁽¹⁾, H. Zargar⁽²⁾, J. Marshall⁽³⁾, T. Rawlinson⁽⁴⁾

⁽¹⁾ Associate Professor, University of Nevada, Reno, klryan@unr.edu

⁽²⁾ Design Engineer, New Millennium Building Systems, hzargar@nevada.unr.edu

⁽³⁾ Associate Professor, Auburn University, jdmarshall@auburn.edu

⁽⁴⁾ Structural Engineer, AECOM, tar629@gmail.com

Abstract

Base isolation systems generally perform well under design-level ground motions to reduce both interstory drift and acceleration demands. During a larger than anticipated earthquake, however, large displacements in the base level may cause pounding between the structure and perimeter moat wall, which can lead to very high acceleration in the superstructure. A phased passive control system, or ‘gap damper’, was conceived to control base isolator displacement during extreme events while having no effect on the isolation system performance for earthquakes up to and including the design level. Providing passive supplemental energy dissipation at a specified gap greater than the design displacement allows the base isolation system to act traditionally in design level events while activating the secondary system in extreme events. Use of this gap damper device eliminates undesirable effects associated with large amounts of supplemental damping at lower intensity motions.

This paper presents the experimental validation of a prototype gap damper developed for practical implementation in a seismically-isolated building. The gap damper device uses four viscous dampers, two in each direction oriented around and attached to a contact surface at one end and a fixed point at the other end. An isolation nub extends down from the base of the building to sit inside the contact surface. An initial gap is provided between the isolation nub outer surface and the inner contact surface. When subjected to earthquake loading, the isolation nub moves within the contact surface and the dampers are not activated until the displacement amplitude exceeds the system initial gap. When the gap is closed, the dampers are activated and impact forces transferred from the isolation nub to the contact system are absorbed.

Shake table testing was performed at the University of Nevada, Reno to simulate the gap damper system functioning within a base isolated building during large motions. Two test configurations consisting of a base isolated building without and with a gap damper system were tested. To the extent possible, the same trials were carried out in both configurations to quantify the influence of the gap damper on isolator displacements and superstructure accelerations compared to the isolated building without a gap damper. The gap damper is found to be more effective in limiting isolator displacements during pulse-type motions compared to long duration cyclic motions, and in predominantly unidirectional motions compared to motions with a strong bidirectional component. In addition, several factors are identified that limited the effectiveness of the gap damper relative to predictions from numerical simulations, which are possible to overcome in the design process. Superstructure accelerations increased as a result of activation of the gap damper, but these high frequency acceleration spikes are not seen to be detrimental to the overall structural performance relative to a conventionally designed building without special seismic protection.

Keywords: Seismic isolation; Phased System; Extreme event.



1. Introduction

Seismic isolation is recognized as one of the best ways to protect a building and its contents from a strong earthquake. The low horizontal stiffness of the isolation system lengthens the fundamental period of the structure, which substantially reduces base shear and resultant structural accelerations. The increased displacement demands are accommodated primarily at the isolation level. Typical seismic isolation devices incorporate energy dissipation mechanisms to limit displacements to an acceptable level, but the inherent damping may not be sufficient to control the displacement during extreme shaking such as a Maximum Considered Earthquake (MCE). Hall et al. [1] numerically simulated the response of an isolated structure subjected to beyond design level ground motions, which raised awareness for the possible consequences such as pounding of the structure against an outer moat wall. In recent years, the community has become increasingly concerned about the performance of seismically-isolated buildings during MCE level earthquakes and beyond. A number of numerical studies have been conducted to predict the response of isolated buildings when subjected to pounding [2-4], and/or predict the statistical likelihood of exceeding certain limit states, including collapse, under rare earthquakes [5-6]. Pounding mitigation measures such as using rubber bumpers as shock absorbers have also been explored [7]. These studies indicate a need to develop reliable methods to limit isolator displacement demands during extreme ground motions and prevent impact with the outer moat wall.

Various approaches for controlling isolator displacements have been investigated. The authors have proposed a passive approach to vary the isolation system damping with ground shaking intensity, based on earlier success with phased systems for different applications [8]. The concept is a phased passive system that triggers additional supplemental damping when a threshold displacement demand is reached. The proposed ‘gap damper’ provides phased behavior by combining a gap element with a hysteretic or viscous energy dissipation device. A physical gap damper device was designed, fabricated and tested to validate the effectiveness of gap damping to reduce isolator displacement demands. The concept adopted for the experimental program is shown in Figure 1. A single gap damper is composed of four energy dissipators – two in each direction – attached to a contact surface that rests on a low friction interface. A stiff member, or “isolation nub” extends down from the base of the building and rests within the contact surface, with a uniform gap on each side. When subjected to an earthquake, the bidirectional motion of the building above the isolation system is projected to the isolation nub. Closure of the gap between the isolation nub and contact surface will cause the contact surface to slide, activating the dampers, which will absorb the impact forces that are transferred from the isolation nub to the contact surface. Fig. 1 illustrates how multiple gap dampers, as needed, could be strategically located between isolation devices at the base of the building. Prior study on the feasibility and optimization of a gap damper has suggested that a gap damper system incorporating a viscous damping mechanism will be most effective in limiting the isolator displacement demands [9]. This study was the basis for the design of the gap damper in the experiment described herein. Results of initial component testing have been reported in [10].

In this paper, the effectiveness of the gap damper system to reduce isolator displacement demands is evaluated based on a shake table test of a one quarter scale base-isolated 3-story steel frame building. The design of system components and the experimental setup is described. Key responses are compared and evaluated for system configurations with and without a gap damper (base isolated alone), and factors that influenced the effectiveness of the gap damper are identified and explained. Also, factors that limited the effectiveness of the gap damper during the experiments compared to theoretical expectations are discussed. The data described in this paper is archived and publicly available in the Network for Earthquake Engineering Simulation (NEES) Project Warehouse [11-12].

2. Experiment Design and Setup

2.1 Overview

For the experiment, a multi-story base-isolated frame was designed to be shaken with and without a gap damper to directly assess the influence of the gap damper on the response. The isolated frame properties were specified for shaking on one of the University of Nevada, Reno (UNR) Earthquake Engineering Laboratory’s biaxial tables. Model to prototype scaling factors were length = 1:4, acceleration = 1:1, and time = 1:2. A one-

bay by one-bay, 3-story steel frame was designed and fabricated. Four lead rubber bearings (LRBs) designed for a previous project [13] were reused to form the isolation system. The gap damper components were custom designed and fabricated for the experiment, including viscous dampers, the contact surface, the isolation nub, and connectors. The total supported structure weight assumed for design was 355.8 kN.

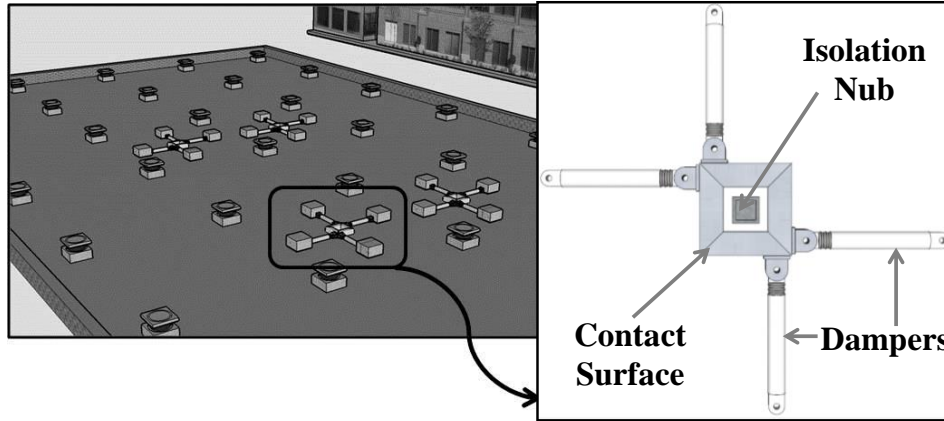


Fig. 1 – Design concept selected for the gap damper implementation, eccentrically oriented dampers attached to a sliding contact surface

The design procedure is summarized as follows. First, a target MCE spectrum with 1.0 s and short-period spectral accelerations $S_{MI} = 1.11 \cdot g$ and $S_{MS} = 2.2 \cdot g$ was scaled for the model domain. Characterized bearing properties and assumed specimen weight were used to identify an approximate displacement demand: $D_{MCE} = 107$ mm. The viscous damper properties were selected based on an equivalent energy dissipation and optimization approach explained in [9]. The dual objectives were to reduce the isolator displacement by 20% from $1.375D_{MCE}$ to $1.1 D_{MCE}$ (to avoid moat wall collision) and to limit the floor acceleration to 3 times those observed in a design earthquake that does not engage the gap damper (displacement $< 0.6D_{MCE}$).

2.2 Isolation System and Gap Damper

A photo of one of the bearings used in gap damper system test is shown in Fig. 2(a). The bearing force-displacement hysteresis loops from the previous test program were used to characterize the properties. A cycle with displacement amplitude of 152 mm – close to the target peak displacement demand for the experiment – was selected for characterization. The isolator properties were determined by fitting a bilinear loop to the recorded hysteresis loop such that the energy dissipated and peak-to-peak effective stiffness of the two loops were equal [Fig. 2(b)]. Table 1 summarizes the characterized bearing properties based on the test data, including the characteristic strength Q_d , post-yield stiffness K_d , and initial stiffness K_i . In the fitting procedure, the relation $K_i = 20K_d$ was assumed. Computed from the characterized bearing properties and the target spectrum, the effective period T and damping ratio ζ are also summarized in Table 1 for three intensities: design displacement, MCE displacement, and the over-moat target displacement for the base isolation configuration ($1.375 \cdot D_{MCE}$). Stability analysis based on the overlapping area method [14] suggested that for the expected axial loads, the bearing displacement should be limited to 102 mm; however, recent studies on bearing stability [e.g., 15] suggest that the overlapping area method to estimate the critical load capacity of bearings is conservative. Therefore, a test plan was developed to cautiously ramp up to an isolator displacement demand of 147 mm.

A single prototype gap damper device was designed and used in both component and system tests [Fig. 3]. The gap damper was assembled from four viscous dampers, a contact surface, and an isolation nub. Each viscous damper was 870 mm in length with a 244.6 kN force capacity and ± 76 mm stroke capacity. The viscous dampers were designed using an equivalent energy dissipation approach and optimization procedure [9, 10]. The dampers with coefficients of 8.14 and 7.13 N·s/m were oriented in the East/West (x) direction and North/South (y) directions, respectively. The contact surface consisted of four HSS 152×152×13 mm members welded at the diagonals to form a square box. The dampers were attached to the contact surface at one end and a reaction support at the other end with pin and clevis connections. The contact surface slid freely on a low friction steel

base plate. The isolation nub was comprised of a 460 mm long 152×152×19 mm built-up box section that was reinforced using four stiffeners (16 mm thick plates).

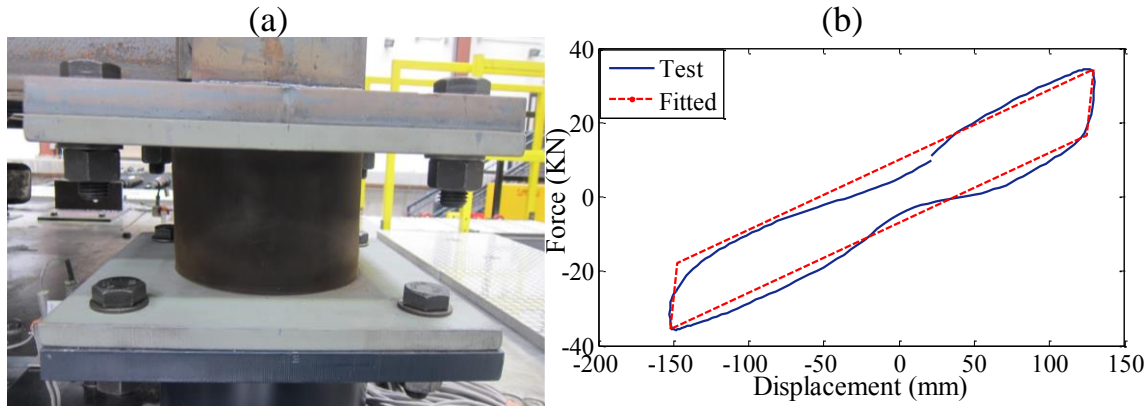


Fig. 2 – (a) Photo of lead-rubber bearing, and (b) bilinear loop fitted to the recorded bearing hysteresis loop for selected cycle

Table 1 – Characterized Properties of Bearings Based on Recorded Hysteresis Loop

Bearing Properties	Value	Effective Properties	Design	MCE	Over-Moat
Characteristic Strength (Q_d)	8.63 kN	Displacement D - mm	53	107	147
Post-yield Stiffness (K_d)	178.6 kN/m	Period T - s	1.02	1.18	1.23
Initial Stiffness (K_i)	357.2 kN/m	Damping Ratio, ζ - %	29.6	19.9	15.6
Yield Disp. (D_y)	2.5 mm				

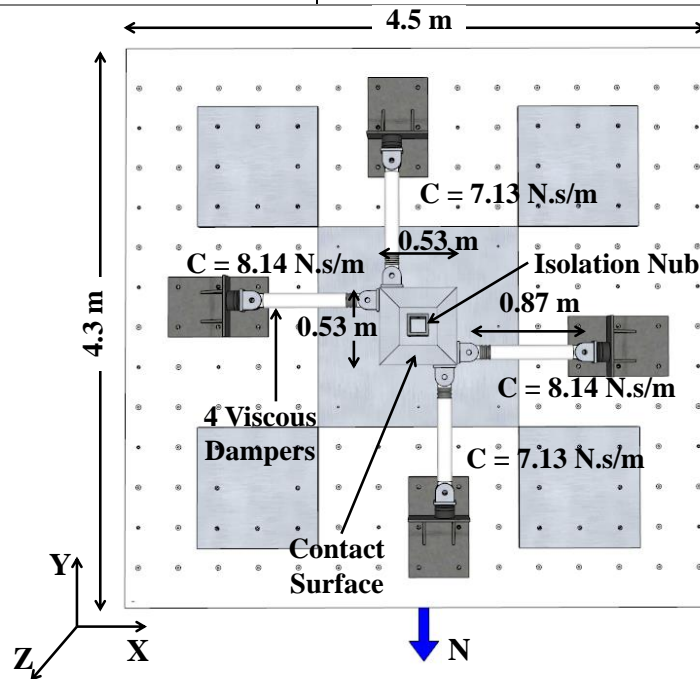


Fig. 3– Gap damper system configuration on shake table

2.3 Steel Frame System and Mass

The 3-story steel frame designed and fabricated for the experiment had the following model dimensions: bay widths = 2.4 m in both directions, story height = 1.2 m, overall frame height = 3.6 m. Lateral resistance was

provided by concentric braces in the North-South direction and moment frames in the East-West direction (Fig. 4). The majority of the specimen mass was provided by supplementary steel plates and lead baskets attached to the frame. Each lead basket was filled with solid lead weights topped with steel plates and constrained by horizontal anchors. The weights on the base, 2nd floor, 3rd floor, and roof were 88.6, 86.2, 87.1 and 77.6 kN, respectively, leading to a total specimen weight of 339.5 kN after the final design was finalized.

The design lateral loads were estimated based on numerical simulation of the simplified structural model with optimized damping coefficient. Using specified geometry and applicable load combinations of ASCE 7-10 [16], the frame was analyzed and designed using SAP 2000. Due to the uncertainty of the impact loading and to ensure safety during the test, all components were designed for a factor of safety of 3 against yielding (demand/capacity ratio $\leq 1/3$). These design assumptions produced a test structure that was much stiffer and stronger than a building designed for code-compliance under comparable seismicity.

2.4 Instrumentation

Instruments were installed to record the desired displacements, accelerations, and forces during the shaking experiments. Load cells installed beneath each bearing measured axial force, shear force in x and y, and moment about x and y directions. Four stringpots attached to the NW and SE bearings and anchored to reference frames on the table measured the bearing displacements in perpendicular directions. For the gap damper configuration, stringpots were attached to each damper in the axial direction to record the damper stroke, and in the orthogonal direction to record the damper transverse displacement. Unidirectional load cells positioned behind each damper recorded the damper axial force. Tri-directional accelerometers, glued to the bottom of the moment frame girders in the NE and SW corners of all floors, recorded the superstructure floor accelerations and the shake table acceleration (for reference). Accelerations on each floor were averaged over the two sensors and filtered using a Butterworth low pass filter with a 25 Hz cutoff frequency. Further details about the instrumentation and data processing are available in [17].

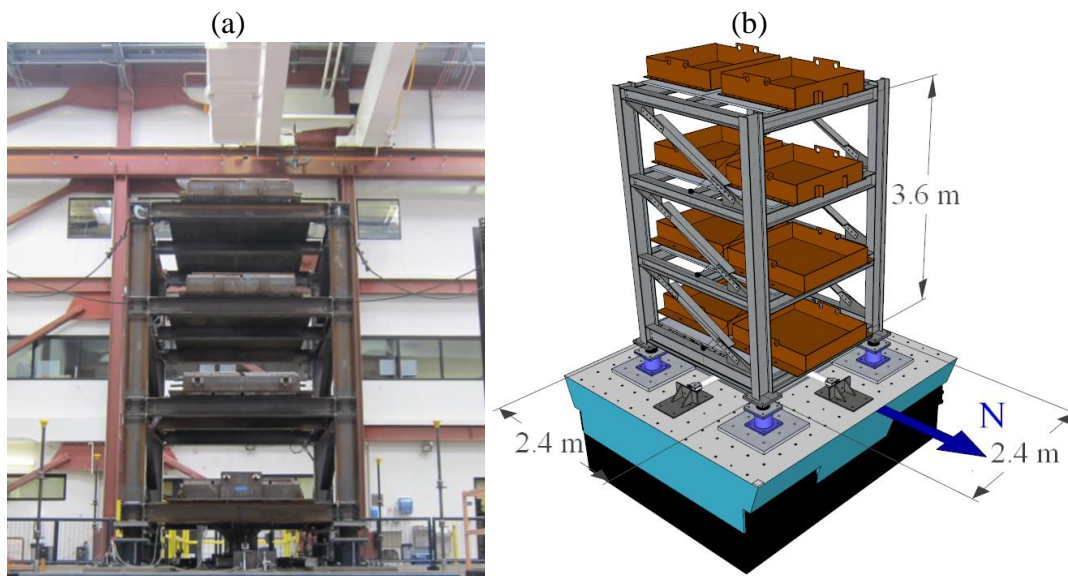


Fig. 4–(a) Photo and (b) 3-dimensional rendering of steel frame specimen assembled on the shake table (lead weights in baskets not shown).

2.5 Selection, Scaling and Sequencing of Input Motions

The test program included the following types of input accelerations: unidirectional sine waves and earthquake records. Two overarching principles governed the selection and scaling of motions, which were: 1) all motions – to the extent possible – were applied identically to both the base-isolated and gap damper configurations, and 2) motions were scaled to target the over-moat isolator displacement of 147 mm in the base-isolated configuration, which was approached safely through a ramp-up sequence of increasing intensities.



The sine wave (SINE) was defined as a harmonic acceleration signal with a 1 s period and amplitude of 0.26 g in its largest of 10 cycles. Three earthquake record horizontal component pairs were selected for both unidirectional and bidirectional tests; for each pair the stronger component was applied during the unidirectional test (see Table 2). The motions recorded during 1989 Loma Prieta at Los Gatos Presentation Center (LGP), 1995 Kobe at Takatori Station (TAK) and 2010 Chile at Concepcion Station (CONC) were selected for this experiment. For SINE and each earthquake record, Table 2 lists the scale factors (X, Y and XY-dir relative to the 100% target) that were successfully applied identically to both base-isolated and gap damper configurations. The earthquake records were generally applied as a three-record sequence with comparable scale factors consistent with the ramp-up plan to reduce the overall test time. The latter two trials in each sequence thus started with a small residual displacement, while the contact surface was recentered after each individual trial or sequence. Further information about the test program including a complete test log is provided in [17].

Table 2 – Trials (Motions and Intensities) Replicated in Base Isolated and Gap Damper Configurations

X-dir	% of Target	Y-dir	% of Target	XY-dir	% of Target
SINE-X	30, 60, 80, 100	SINE-Y	60, 80, 100	-	-
LGP-X	40, 60, 70	LGP-Y	60	LGP-XY	40, 60, 80, 100
TAK-X	40, 60, 80, 100	TAK-Y	60, 80	TAK-XY	40, 60, 80, 100
CONC-X	40, 60, 80, 100	CONC-Y	60, 80	CONC-XY	33, 49, 66, 80, 100

3. Gap Damper System Test Results

3.1 Summary of Test Results

The effectiveness of the gap damper system is examined by comparing the bearing lateral displacements and base and roof level accelerations observed for the suite of motions applied to both base-isolated and gap damper system configurations. A displacement reduction factor (*% Reduction*) of the peak bearing displacement in the gap damper relative to the base isolation configuration was computed as follows:

$$\% \text{ Reduction} = 100 * \left(\frac{D_{BI} - D_{GD}}{D_{BI}} \right) \quad (1)$$

where D_{BI} and D_{GD} are peak displacements observed in any isolator in the base-isolated and gap damper configurations, respectively. Fig. 5 presents the displacement reduction factor [Eq. (1)] as a function of intensity scaling factor for the different motions considered in the test program. The markers represent individual trials; an open marker indicates the gap damper was not activated. For x-direction trials [Fig. 5(a)], the displacement reduction factor generally (with the exception of CONC-X) increased with increasing intensity scaling factor, which means that the gap damper system was more effective at reducing the displacement for larger intensity motions. During the largest intensity x-direction SINE (100%), LGP (70%), and TAK motions (100%), displacement reductions of 9.2%, 15.2% and 13.9% were observed. The peak x-direction bearing displacements ranged from 127.5 mm to 148.6 mm. Displacement reduction factors at peak scaling intensities in the y-direction ranged from 4.4% to 10.5%. In both x and y-directions, the gap damper system was not effective in reducing the peak displacement for the CONC motion. For bidirectional trials [Fig. 5(c)], peak resultant displacements in the base isolation configuration at 100% intensity were near 142 mm for all motions. Reductions in displacement due to the gap damper were observed only for LGP (reduction factor of 10% at 100% scaling intensity); displacements increased in the gap damper configuration for both TAK and CONC motions. Generally, during bidirectional motions with strong displacement demands in both x and y-directions (e.g. TAK), the gap damper system was not as effective in reducing the displacement.

As illustrated here, the observed displacement reduction induced by the gap damper system was lower than the 20% targeted during design for all motions (e.g. 15% for LGP-X). Fig. 6 illustrates force vs displacement in the NE and SW bearings (compared for the two test configurations) as well as the East and West

dampers during the largest cycle of LGP-X 70%. The energy dissipation of each component over the selected cycle is also indicated. The reduction in isolator displacement [Fig. 6(a), 6(b)] is apparent in the bearing force-displacement loops, but the effective yield force and size of the loop decreased at the smaller displacements, which means that less energy was dissipated by the isolator than theoretically accounted for during design. The damper force-displacement loops show the activation of the damper when the gap is closed, at about 64 mm in +x but 0 mm in -x due to the translation of the contact surface. The initial slope of the damper force-displacement indicates a flexibility associated with damper activation, whereas a perfectly rigid gap element was numerically assumed. Finally, note that the viscous damper damping coefficients were lower than expected due to loss of the damper preload. These factors likely contributed to the shortfall in the observed relative to predicted displacement reduction.

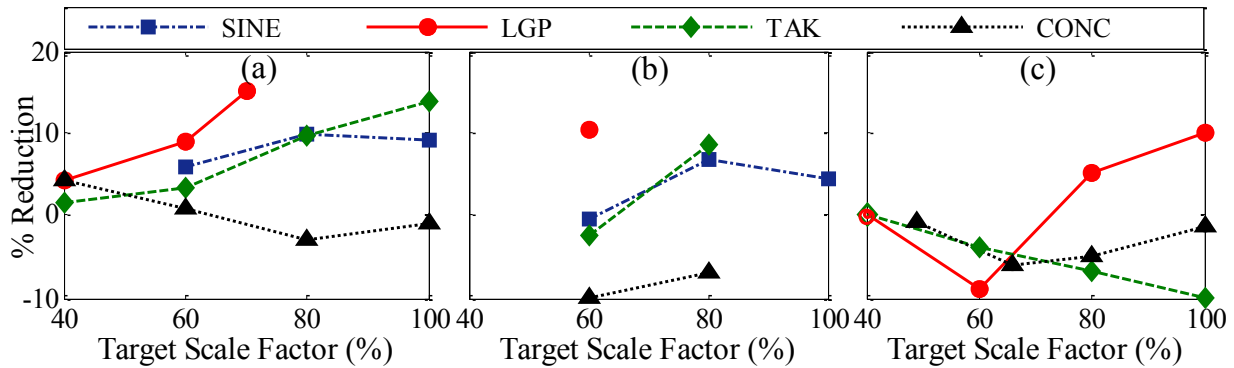


Fig. 5–Reduction of peak horizontal displacement due to gap damper system vs intensity scaling factor during: (a) unidirectional (x-dir) (b) unidirectional (y-dir) and (c) bidirectional motions.

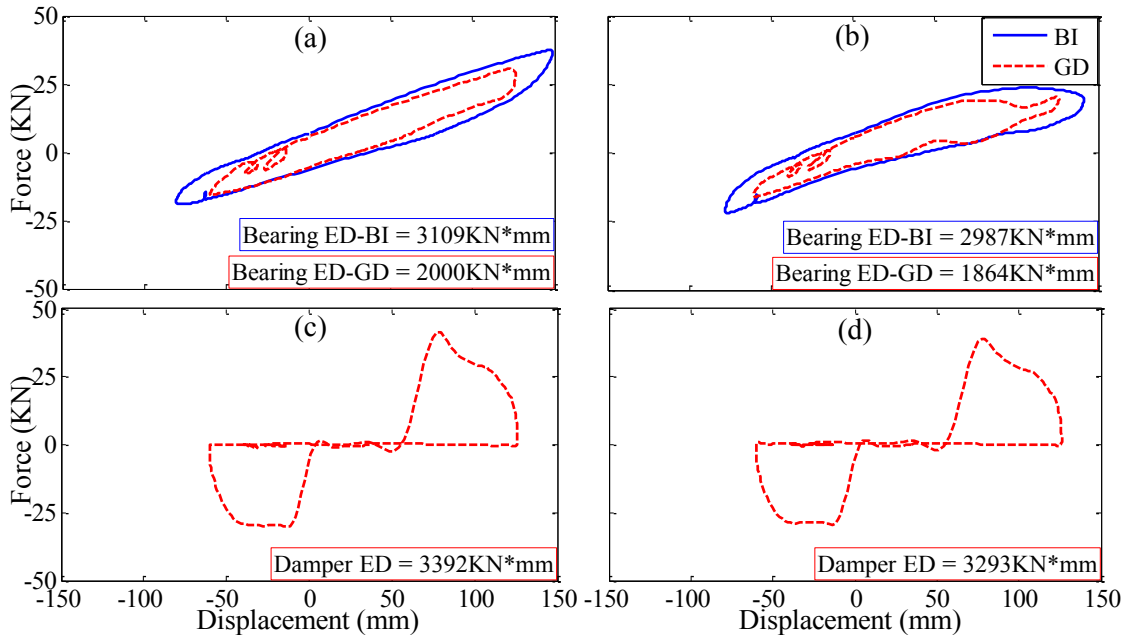


Fig. 6–Largest cycle force vs displacement in (a) SE bearing, (b) NW bearing, (c) East damper, and (d) West damper during LGP-X 70%

An acceleration ratio ($Ratio-A_x$), which represents the amplification of peak floor acceleration at a given location in the gap damper configuration relative to the base isolation configuration, was computed as

$$Ratio-A_x = \frac{A_{x-GD}}{A_{x-BI}} \quad (2)$$

where A_{X-BI} and A_{X-GD} are x-direction floor accelerations in the base-isolated and gap damper configurations, respectively. (Accelerations observed in the y-direction were similar.) Base and roof acceleration ratios as a function of intensity scaling factor for the different motions in the test program are illustrated in Fig. 7. An acceleration ratio = 1.0 means the gap damper was not activated in the x-direction. Larger acceleration ratios were consistently observed at the base level compared to the roof level. Due to the local impact effect, the base acceleration ratio varied widely from 1 to 4.5, while the range of the roof acceleration ratio was limited to 1 to 2.5. Acceleration ratios increased with increasing intensity scaling, more so for base acceleration than for roof acceleration. Acceleration ratios were similar for unidirectional motions [Fig. 7(a), 7(c)] and bidirectional motions [Fig. 7(b), 7(d)]. 1.18 g was the largest superstructure acceleration observed at the base level, which should not be of the intensity to cause structural or even much nonstructural damage. Fig. 7 also indicates the range of realized isolator displacement as a function of D_{MCE} in the base-isolated configuration for each target scale factor. This shows that floor accelerations are amplified even for motions that would not have reached D_{MCE} , which is a drawback to the gap damper system.

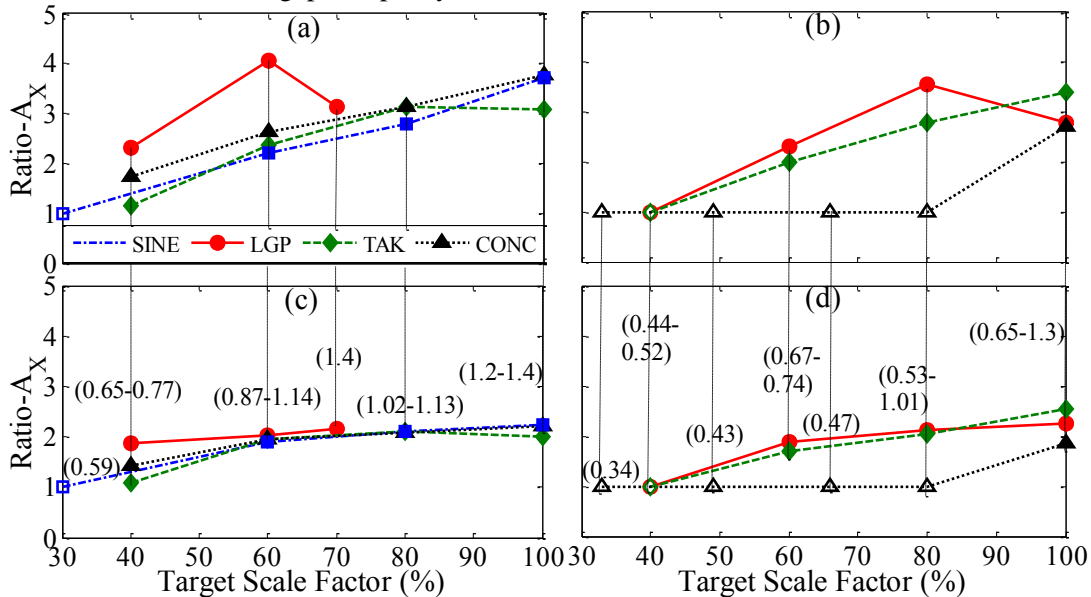


Fig. 7–X-direction acceleration ratio vs intensity scaling factor of: base level during (a) unidirectional (x-dir) and (b) bidirectional motions; and roof level during (c) unidirectional (x-dir) and (d) bidirectional motions. Labels indicate range of realized displacement in base-isolated configuration, as a fraction of D_{MCE} .

3.2 Cyclic Effects

The CONC motion was recorded during a long duration subduction earthquake that produced many cycles of strong shaking, distinguishing it from the near-fault TAK and LGP motions that were dominated by a single fling pulse. The cyclic response characteristics observed in the LGP and CONC motions are compared to provide further insight of the system dynamics. Fig. 8 illustrates the x-direction NW bearing displacement and velocity histories (derived by numerical differentiation of the damper stroke using a backward difference approximation) and the West damper displacement history during LGP-X 70% and CONC-X 100%.

During LGP-X 70%, the cycle producing the largest displacement demand [Fig. 8(a)] coincided with the first gap damper activation [Fig. 8(e)]. The gap damper was centered with a gap of 63.5 mm on all sides when activated in this cycle. The velocity upon damper activation was likely close to the bearing peak velocity of 799.3 mm/s [Fig. 8(c)], and produced a large stroke of 59.6 mm across the damper [Fig. 8(e)]. In contrast, during CONC-X 100%, the gap damper system was activated several times [Fig. 8(f)] as the motion intensity built up to the peak isolator displacement [Fig. 8(b)]. During the first full cycle, the displacement demand was reduced in the presence of the gap damper. However, in the second cycle, the displacement amplitude continued to build up and no reduction in the bearing displacement was observed. Due to asymmetries in the damper stroke in the positive and negative direction [Fig. 8(f)], the displacement history of the NW bearing displacement shifted in the negative direction compared to that for base isolation alone, which may have contributed to a larger negative

displacement peak. In summary, the gap damper system was more effective in reducing displacements during motions with a single large cycle compared to motions that gradually build up to a peak intensity.

3.3 Unidirectional versus Bidirectional Excitation

According to Fig. 5, the displacement reduction was highly variable and the gap damper system was generally less effective for bidirectional trials. Fig. 9 compares the NW bearing displacement traces (displacement in x-direction vs. displacement in y-direction) in the base-isolated and gap damper configurations during LGP-XY 100% and TAK-XY 100%. The gap damper reduced the displacement by 10% compared to isolation alone for LGP-XY 100% [Fig. 9(a)], but did not reduce displacement for Kobe-XY 100% [Fig. 9(b)]. LGP consisted of one strong and one weak component which led to a large bearing displacement demand in the x-direction [139 mm peak in the base-isolated configuration] compared to small y-direction displacement demands [45.7 mm peak]. Therefore, the bearing moved predominantly in the x-direction [Fig. 9(a)]. In contrast, both components of TAK were strong, which led to the bearing reaching its peak displacement along a diagonal [Fig. 9(b)]. Classifying the LGP motion as effectively unidirectional and the TAK motion as bidirectional, the evidence suggests that the gap damper system is considerably more effective for unidirectional motions. The isolation nub can move up to 89 mm in a 45° diagonal direction compared to 63.5 mm in a horizontal direction (an increase of 40%) before reaching the contact surface. Activating the gap damper at a larger displacement relative to the target limited the ability to reduce the isolator displacement.

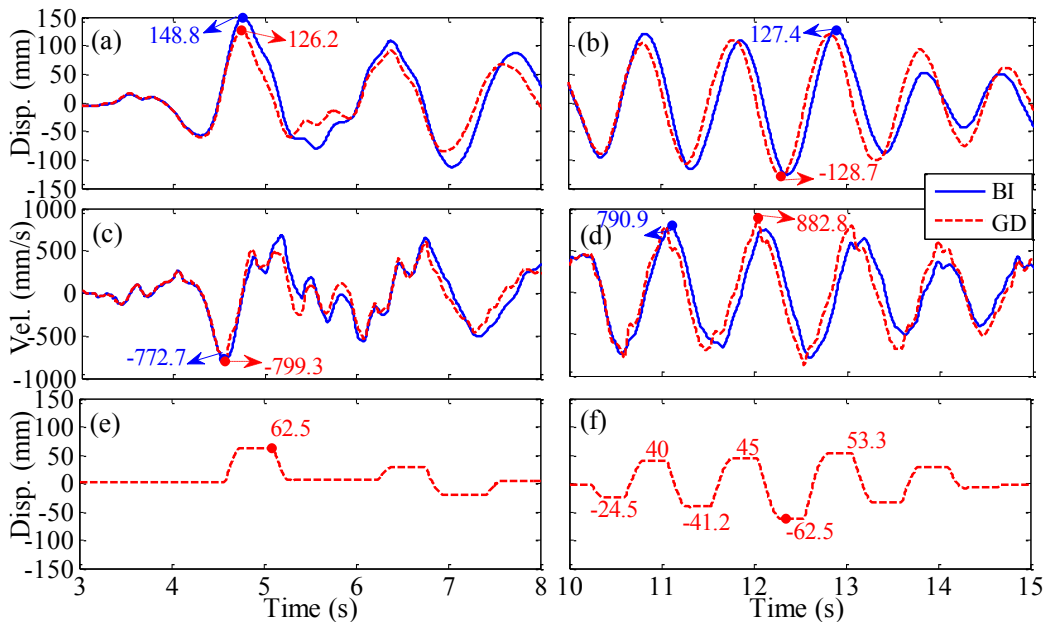


Fig. 8—(a)-(b) NW bearing displacement history, (c)-(d) NW bearing velocity history, and (e)-(f) displacement history across East damper in x-direction during LGP-X 70% and CONC-X 100%

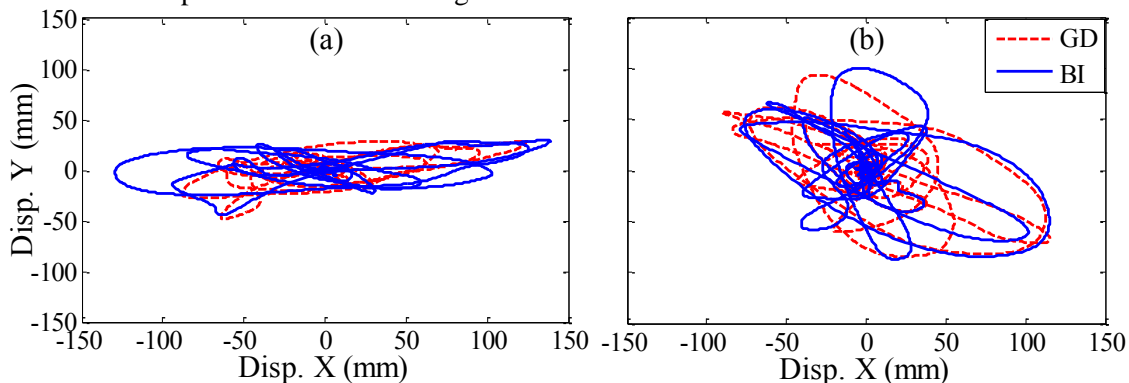


Fig. 9—NW bearing displacement trace in the base-isolated (BI) and gap damper (GD) configurations during: (a) LGP-XY 100% and (b) TAK-XY 100% trials

The impact angle is also believed to reduce the effectiveness of the gap damper in bidirectional motions. Fig. 9(b) shows that during the strongly bidirectional TAK motion, the NW bearing, and by association the isolation nub, moved mainly in a circular or diagonal direction. At the instant the isolation nub first impacted the contact surface, the bearing was oriented at 42° with respect to the x-direction. On the cycle of the peak displacement, the nub impacted at 30° and slid along the contact surface rather than sustain hard impact.

4. Factors that Limited the Experimental Gap Damper Effectiveness

4.1 Bearing Instability

During some motions for the gap damper system test, unusual localized loss of strength in the bearing hysteresis loops was observed. This localized loss of strength imposed large horizontal displacement demand on the bearings. Fig. 10 presents select x-direction responses of the NW bearing during the cycle of the bearing peak displacement for the LGP-X 70% motion. In the NW bearing hysteresis loop [Fig. 10(a)], localized loading and unloading of the bearing was observed (area enclosed by green rectangle). A localized loss of strength was also observed in the bearing hysteresis loop at displacement ranging between 102 mm to 127 mm during the trial with gap damper system. The localized loss of strength is enclosed by a blue circle [Fig. 10(a)], and corresponds to the peak bearing displacement and shear force at 4.76 s [Fig. 10(b), 10(c)].

The bearing axial force history [Fig. 10(d)] provides insight as to why a localized loss of strength occurred in the NW bearing only during the trial with gap damper system. The NW bearing experienced a peak compressive force of 211.2 kN at 4.65 s during this trial [Fig. 10(d)], which corresponded to horizontal displacement of 102 mm at the start of the localized loss of strength. Therefore, the observed localized loss of strength was due to a bearing instability resulting from the combination of large compression force and lateral displacement demand that was unique to the gap damper configuration. Axial force variation in the bearings due to overturning was expected, but Fig. 10(d) shows additional localized axial force variation in the gap damper configuration. In particular, a large axial force spike (increasing axial force in the bearing) was timed with the damper activation at 4.65 s. Therefore, the impact force upon gap damper activation appears to induce additional overturning that is manifested as increasing axial force demand on the bearings.

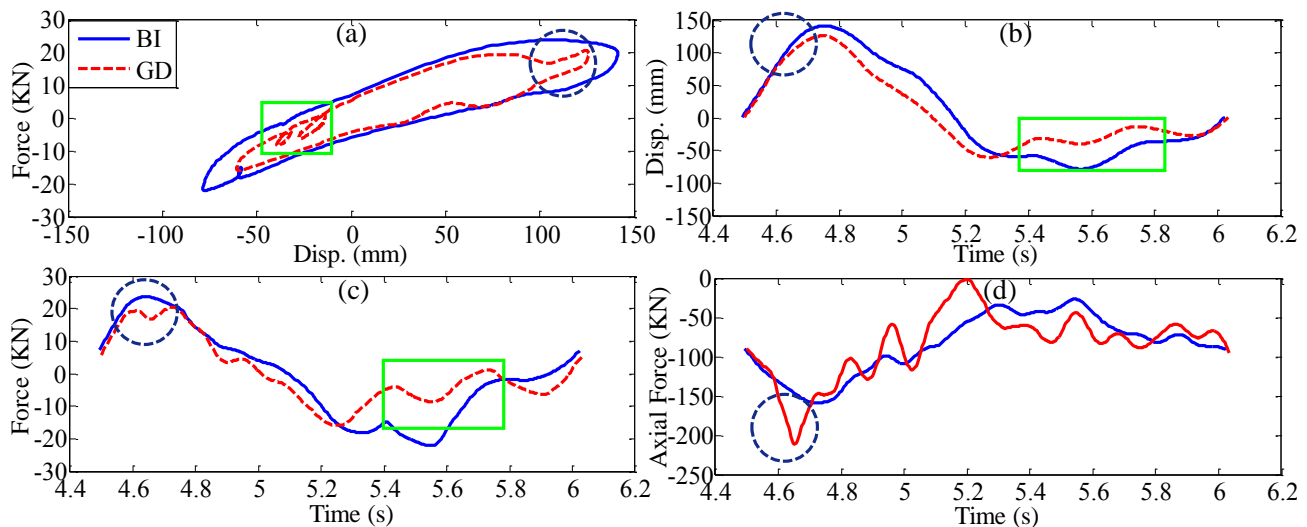


Fig. 10–For peak bearing cycle: (a) bearing force vs. displacement, (b) displacement history, (c) shear force history and (d) axial force history for NorthWest bearing, during LGP-X 70% in x-direction

The localized loss of strength due to bearing instability affected the gap damper performance in two ways. First, the energy dissipation provided by the bearings was reduced since the enclosed area of the bearing shear force versus displacement loop decreased. Less energy dissipation leads to larger displacement demands on bearings. Also, once the instability limit was reached in a bearing, there was no instantaneous stiffness to resist the bearing movement. So, the bearing instability that leads to increasing bearing displacements can work

against the gap damper potential to reduce bearing displacement. This effect can be mitigated in real applications by designing the bearings to have sufficient reserve capacity to sustain the level of displacement associated with the gap damper activation.

4.2 Bearing Degradation

To investigate the consistency of the bearing response over the test program, some trials without the gap damper system were repeated at the end of the test program. LGP-X 60% is presented here as a sample repetition trial. Fig. 11 presents and compares the SE and NW bearing shear force versus horizontal displacement history during LGP-X 60% and LGP-X 60% - Repeat trials. During the repetition, the peak displacement increased by 3.3 mm (2.7%) in the SE bearing and 12.7 mm (10.7%) in the NW bearing [Fig. 11]. From the hysteresis loops, the energy dissipation provided by the bearings was reduced during the repetition compared to the same cycle in the original trial. The bearing hysteresis loops suggest that bearing strength and stiffness may have gradually decreased over the course of the experiments. These changes in bearing properties led to a longer effective period and smaller hysteresis loops (smaller damping ratio) for trials later in the test sequence, which included the gap damper trials. In general, the gap damper system performance will be affected by bearing degradation if the response during an excitation is sensitive to changes in stiffness and damping.

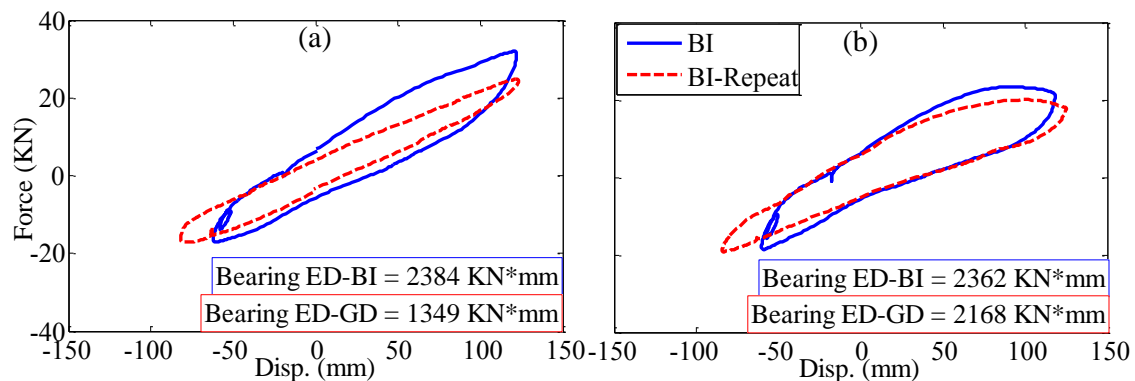


Fig. 11–Bearing peak cycle hysteresis loops: (a) SE and (b) NW subjected to LGP-X 60% and LGP-X 60% - Repeat

5. Conclusions

In this study, the effectiveness of the gap damper to reduce isolator displacement demands in extreme earthquakes was experimentally evaluated during shake table testing of a quarter scale base-isolated frame. Displacements were reduced by up to 15% relative to the configuration with base isolation. Superstructure floor accelerations increased by factors ranging from 2 to 4 due to damper activation, but were limited to a peak of about 1.18g over the whole test program. Several factors influenced the effectiveness of the gap damper.

- The gap damper is more effective in reducing displacements during motions with a single large cycle compared to motions that build up to a peak intensity over several cycles.
- The gap damper is significantly more effective for unidirectional motions, or motions with a strong unidirectional component, compared to strongly bidirectional motions, because the gap damper activates at a larger displacement when the base moves diagonally rather than along a single axis.
- Bearing instability and degradation were found to limit the gap damper system performance observed in the experiment by decreasing the energy dissipated in the bearing hysteresis loops. These factors tended to increase bearing displacements and counteracted the gap damper potential for displacement reduction.

This was the first implementation of a phased damping concept as a backup system to control isolator displacements during very large intensity motions, which could mitigate concerns about the fate of isolated structures during beyond-MCE events. The following would be required before practical implementation of a gap damper is possible: 1) improvement on the physical design of the gap damper, and 2) reliable simulation of



the influence of gap damper activation on the structural acceleration, as compared to impact against a hard stop (moat wall).

6. Acknowledgement

This research was supported by National Science Foundation through Grants No. CMMI-1101105 and CMMI-1100922. This support is gratefully acknowledged. Any opinions, findings, conclusions, or recommendations expressed in this material are those of the authors and do not necessarily reflect the views of the National Science Foundation.

7. References

- [1] Hall JF, Heaton TH, Halling, MW, Wald DJ (1995): Near-source ground motion and its effects on flexible buildings. *Earthquake Spectra*, **11** (4), 569-605.
- [2] Tsai HC (1997): Dynamic analysis of base-isolated shear beams bumping against stops. *Earthquake Engineering and Structural Dynamics*, **26**, 515-528.
- [3] Komodromos P, Polycarpou PC, Papaloizou L, Phocas MC (2007): Response of seismically isolated buildings considering poundings. *Earthquake Engineering & Structural Dynamics*, **36** (12), 1605-1622.
- [4] Pant DR, Wijeyewickrema AC (2012): Structural performance of a base-isolated reinforced concrete building subjected to seismic pounding. *Earthquake Engineering and Structural Dynamics*, **41** (12), 1709-1716.
- [5] Qu Z, Kishiki S, Nakazawa T (2013): Influence of isolation gap size on the collapse performance of seismically base-isolated buildings. *Earthquake Spectra*, **29** (4), 1477-1494.
- [6] Cutfield MR, Ryan KL, Ma Q (2015): Comparative life cycle analysis of conventional and base-isolated buildings. *Earthquake Spectra*, In Press. doi: <http://dx.doi.org/10.1193/032414EQS040M>.
- [7] Polycarpou PC, Komodromos P (2011): Numerical investigation of potential mitigation measures for poundings of seismically isolated buildings. *Earthquakes and Structures*, **2** (1), 1-24.
- [8] Marshall JD, Charney FA (2010): A hybrid passive control device for steel structures I: development and analysis. *Journal of Constructional Steel Research*, **66** (10), 1278-1286.
- [9] Zargar H, Ryan KL, Marshall JD (2013): Feasibility study of a gap damper to control seismic isolator displacements in extreme earthquakes. *Structural Control and Health Monitoring*, **20** (8), 1159-1175.
- [10] Rawlinson TA, Marshall JD, Ryan KL, Zargar H (2015): Development and experimental evaluation of a passive gap damper device to prevent pounding in base-isolated structures. *Earthquake Engineering and Structural Dynamics*, **44** (11), 1661-1675.
- [11] Zargar H, Ryan KL (2015): System Test of a Base-Isolated Building. Network for Earthquake Engineering Simulation (distributor), Dataset, DOI:10.4231/D37W67661.
- [12] Zargar H, Ryan KL (2015): System Test of a Base-Isolated Building with Gap Damper. Network for Earthquake Engineering Simulation (distributor), Dataset, DOI:10.4231/D3445HD26.
- [13] Monzon EV, Buckle IG, Itani AM (2013): Seismic Performance of Curved Steel Plate Girder Bridges with Seismic Isolation. *CCEER Report No. 13-06*, Center for Civil Engineering Earthquake Research, University of Nevada, Reno, NV.
- [14] Buckle IG, Liu H (1993): Stability of elastomeric seismic isolation systems Proc., Seminar on Seismic Isolation, Passive Energy Dissipation and Control, ATC-17-1, Applied Technology Council, Calif., 293-305.
- [15] Weisman J, Warn GP (2012): Stability of elastomeric and lead-rubber seismic isolation bearings. *Journal of Structural Engineering*, **138** (2), 215-223.
- [16] ASCE/SEI. Minimum Design Loads for Buildings and Other Structures: ASCE Standard 7-10 2010; Reston, VA.
- [17] Zargar Shotorbani H, Ryan KL (2015): Analytical and Experimental Study of Gap Damper System to Limit Seismic Isolator Displacements in Extreme Earthquakes. *CCEER Report No. 15-04*, Center for Civil Engineering Earthquake Research, University of Nevada, Reno, NV.